THE ASTROPHYSICAL JOURNAL, 563:229–238, 2001 December 10

X-RAY OBSERVATIONS OF XTE J1550−564 DURING THE DECAY OF THE 2000 OUTBURST. I. *CHANDRA* AND *RXTE* ENERGY SPECTRA

JOHN A. TOMSICK
Center for Astrophysics and Space Sciences, University of California at San Diego, MS 0424, La Jolla, CA 92093; jtomsick@ucsd.edu
STÉPHANE CORBEL
Université Paris VII and Service d'Astrophysique, Centre d'Etudes de Saclay, F-91191 Gif sur Yvette Cedex, France; corbel@discovery.saclay.cea.fr
AND
PHILIP KAARET
Harvard-Smithsonian Center for Astrophysics, 60 Garden Street, Cambridge, MA 02138; pkaaret@cfa.harvard.edu
Received 2001 May 2; accepted 2001 August 7

ABSTRACT

We report on the evolution of the X-ray energy spectrum for the black hole candidate (BHC) X-ray transient XTE J1550−564 during the decay of the 2000 outburst. The *Rossi X-Ray Timing Explorer* (*RXTE*) and *Chandra* observations span nearly 5 orders of magnitude in luminosity. The *RXTE* spectra are dominated by a power-law component, and a comparatively weak soft component was also detected for the first two observations. The source made a transition to the canonical hard state near a luminosity of 9×10^{36} ergs s^{-1} over several observations, as evidenced by a drop in the flux of the soft component in the *RXTE* energy band and a hardening of the power-law component to a photon index near 1.6. The power law did not exhibit this behavior for the previous XTE J1550−564 outburst. For some observations, we detect a high-energy cutoff and find that the cutoff is more significant and at lower energy during the transition than in the hard state. The cutoff in the hard state is at higher energy than has been seen for most previous accreting BHCs. The *Chandra* spectrum provides evidence for spectral evolution after the hard-state transition. It is well, but not uniquely, described by a power law with a photon index of $2.30^{+0.41}_{-0.48}$ (90% confidence) and interstellar absorption. Advection-dominated accretion flow models predict gradual spectral softening as the luminosity drops, but our observations do not allow us to determine whether the spectral evolution is gradual or sudden. The lowest luminosity we measure for XTE J1550−564 with *Chandra* is 5×10^{32} ergs s^{-1} (0.5–7 keV, for a distance of 4 kpc). Although this is probably not the true quiescent luminosity, it represents a useful upper limit on this quantity.

Subject headings: accretion, accretion disks — black hole physics — stars: individual (XTE J1550−564) — X-rays: bursts — X-rays: stars

1. INTRODUCTION

The energy spectra of accreting black hole candidates (BHCs), while complex, are dominated by two emission components: a soft thermal component peaking below 10 keV and a hard component that extends to hundreds of keV (Grove et al. 1998). For most BHC X-ray transients, both components are present in the X-ray band when the source is bright during the outburst, and the source is said to be in the soft state or the very high state depending on the details of the spectral and timing properties (see van der Klis 1995 for a review of spectral states). There is strong evidence that the soft component is optically thick blackbody emission from the accretion disk. As the X-ray luminosity drops, significant changes in the spectral and timing properties are observed as sources enter the hard state. The soft component becomes undetectable at energies above 1 keV, and the spectrum is dominated by a hard power law or breaking power-law component. An increase in the strength of the timing noise is also characteristic of the transition to the hard state. It is likely that the high-energy emission is due to inverse Comptonization of soft photons by energetic electrons, but there is uncertainty about the system geometry, the electron energy distribution, and the mechanism for transferring energy to the electrons. One possibility is that a quasi-spherical, optically thin region forms in the inner portion of the accretion disk as predicted by advection-dominated accretion flow (ADAF) models (Narayan, Garcia, & McClintock 1997). Another possibility that implies a different site for hard X-ray production is that the hard X-ray emission is due to magnetic flares above the disk (Galeev, Rosner, & Vaiana 1979). The source behavior during the decay from the hard state into quiescence is not well established. Here we present a study of the evolution of the energy spectrum for the BHC X-ray transient XTE J1550−564 spanning nearly 5 orders of magnitude in luminosity during outburst decay.

XTE J1550−564 was first detected by the *Rossi X-Ray Timing Explorer* (*RXTE*) All-Sky Monitor (ASM) in 1998 September (Smith 1998). It was identified as a probable black hole system based on its X-ray spectral (Sobczak et al. 1999) and timing properties. The source shows strong aperiodic variability including low- (0.08–18 Hz) and high- (100–285 Hz) frequency quasi-periodic oscillations (Cui et al. 1999; Remillard et al. 1999; Homan, Wijnands, & van der Klis 1999; Remillard et al. 2001; Homan et al. 2001; Miller et al. 2001b). The optical (Orosz, Bailyn, & Jain 1998) and radio (Campbell-Wilson et al. 1998) counterparts were identified, and recent optical observations confirm that the system contains a black hole (Orosz et al. 2001). A superluminal ejection was observed in the radio (Hannikainen et al. 2001), establishing that the source is a microquasar similar to GRO J1655−40 and GRS 1915+105. XTE

J1550−564 became active in X-rays again in 2000 April (Smith et al. 2000), making it one of the few BHC X-ray transients for which multiple outbursts have been observed. X-ray observations during the 2000 outburst were made by us as well as by another group (Miller et al. 2001a). A radio study of the 2000 outburst (Corbel et al. 2001) showed evidence for a compact jet when the source was in the hard state and that this jet is quenched during the intermediate/very high state (see Homan et al. 2001 for a discussion of spectral states in XTE J1550−564). In 2001 January, the source flared again and was detected in the X-ray (Tomsick et al. 2001), optical (Jain, Bailyn, & Tomsick 2001), and radio, but this flare did not develop into a full outburst.

In this paper, we focus on the properties of the energy spectrum during the decay of the 2000 outburst. The *RXTE* and *Chandra* observations used for this paper include a study of a transition to the hard state and spectral evolution at low luminosities. A study of the timing properties using the *RXTE* data is presented in a companion paper (Kalemci et al. 2001, hereafter Paper II).

2. OBSERVATIONS AND LIGHT CURVE

During the XTE J1550−564 outburst, we obtained two *Chandra* observations of the BHC at low flux and several observations with *RXTE* during the decay of the outburst. The *RXTE* observations were made under a program to study BHC X-ray transients during outburst decay, and the *Chandra* observations were granted from Director's Discretionary Time, motivated by our *RXTE* observations. Figure 1 shows the 1.5–12 keV light curve for the outburst, including data from the *RXTE*/ASM and our pointed observations. Table 1 provides information about the observations that we used for spectral analysis.

When observing sources near the Galactic plane with *RXTE*, one must be aware of contributions from the Galactic ridge emission (Valinia & Marshall 1998) and the possibility of source confusion. XTE J1550−564 is 1°.8 from the Galactic plane, and the Galactic ridge emission is significant for our fainter observations. To estimate the level of Galactic ridge emission, we used public *RXTE* observations of the XTE J1550−564 position that were made when the source was in quiescence. The observations were made on 1999 August 13 and consist mostly of scans used to study the nearby supernova remnant G326.3–1.8. Although the observations include only 128 s on the XTE J1550−564 position, this is sufficient to determine the X-ray flux. Assuming an absorbed Raymond-Smith plus power-law model with the parameter values found by Valinia & Marshall (1998) for the central ridge but with the overall normalization left as a free parameter, the Galactic ridge flux is 1.68×10^{-11} ergs cm^{-2} s^{-1} (1.5–12 keV) at the XTE J1550−564 position.

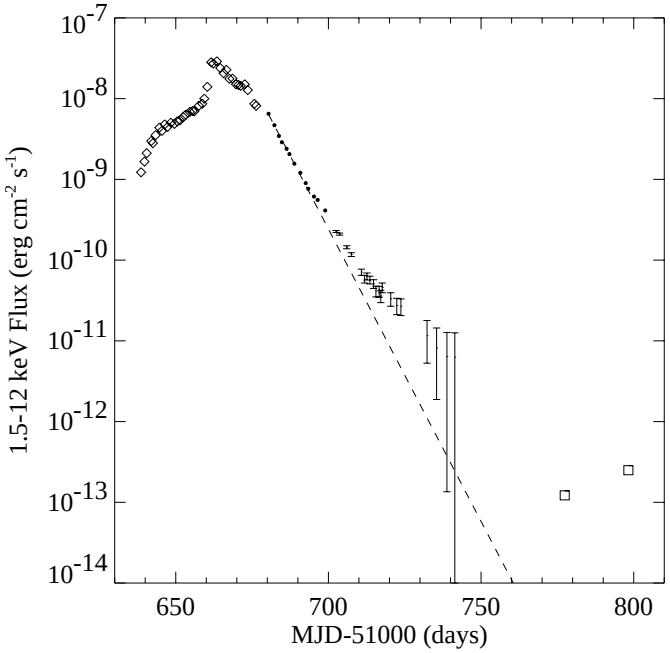

FIG. 1.—The X-ray light curve for the 2000 outburst from XTE J1550−564, including data from the *RXTE*/ASM (*diamonds*), *RXTE* pointed observations (*filled circles and error bars*), and *Chandra* observations (*squares*). Dashed line is an exponential decay with an *e*-folding time of 6.0 days.

TABLE 1

RXTE OBSERVATIONS OF XTE J1550−564

Observation	MJD[a]	Integration Time (s)	PCUs[b]	PCA Count Rate[c] (counts s^{-1})	HEXTE Count Rate[d] (counts s^{-1})	Flux[e]
1	51,680.391	2032	2, 3, 4	1992	36	5.6×10^{-9}
2	51,682.316	1712	2, 3, 4	1575	40	4.7×10^{-9}
3	51,683.786	2688	2, 3, 4	1278	40	4.0×10^{-9}
4	51,684.769	848	1, 2, 3, 4	1145	38	3.5×10^{-9}
5	51,686.302	1520	1, 2, 3, 4	955	33	3.0×10^{-9}
6	51,687.229	1408	2, 3	855	30	2.7×10^{-9}
7	51,688.846	1712	2, 3	663	24	2.1×10^{-9}
8	51,690.807	1760	2, 3	508	17	1.6×10^{-9}
9	51,692.562	1728	2	380	13	1.2×10^{-9}
10	51,693.411	1168	2	330	12	1.0×10^{-9}
11	51,695.271	1136	2, 3	258	9	8.1×10^{-10}
12	51,696.483	1712	2, 3, 4	218	8	7.1×10^{-10}
13	51,698.948	1152	2	165	6	5.0×10^{-10}

[a] Modified Julian Date (MJD = JD − 2,400,000.5) at the midpoint of the observation.
[b] The Proportional Counter Units (other than PCU 0) that were on during the observation.
[c] The 3–25 keV count rate normalized to the rate for 5 PCUs (all three layers) after background subtraction.
[d] The 18–150 keV count rate for HEXTE (cluster A only) after background subtraction.
[e] Absorbed 3–25 keV flux in units of ergs cm^{-2} s^{-1}.

Source confusion is also an issue for our *RXTE* observations. The transient pulsar XTE J1543−568 (Marshall, Takeshima, & in't Zand 2000), which is 0.°966 from the XTE J1550−564 pointing position (Kaptein, in't Zand, & Heise 2001), was in outburst during our observations. We analyzed the ASM data for XTE J1543−568 to determine the flux this source contributed during our observations. For ten 15 day intervals during the XTE J1550−564 outburst, the ASM count rate for the pulsar was between 0.15 and 0.90 counts s^{-1}. At the maximum count rate and given the 3% response that is expected for the angular separation, we estimate that XTE J1543−568 contributed a flux of 1.08×10^{-11} ergs cm^{-2} s^{-1} (1.5–12 keV) during our observations. The level of emission observed during our last two *RXTE* observations is consistent with the emission coming from the Galactic ridge and XTE J1543−568 with little or no contribution from XTE J1550−564. The emission properties observed for our last several observations confirm that we are seeing significant contributions from the Galactic ridge and XTE J1543−568. We find a strong iron line at 6.7 keV for our last several observations, which is a property of the Galactic ridge emission (Valinia & Marshall 1998). Also, we detect pulsations at 27 s, which is the known pulse period for XTE J1543−568 (Marshall, Takeshima, & in't Zand 2000).

For the light curve shown in Figure 1 we assume that the flux contribution to the *RXTE* observations from the Galactic ridge emission and XTE J1543−568 is between 1.68×10^{-11} ergs cm^{-2} s^{-1} and the value we find for our last observation, 2.94×10^{-11} ergs cm^{-2} s^{-1} (1.5–12 keV). For the first 13 *RXTE* observations, the level of contamination is not significant. These observations are shown as filled circles in Figure 1, and we use only these observations for the spectral analysis described below. Error bars are shown for the other *RXTE* observations. Fitting an exponential to the first 13 *RXTE* observations gives 6.0 days for the *e*-folding time for the decay, which is a very fast decay compared to other BHC X-ray transients (Chen, Shrader, & Livio 1997; Tomsick & Kaaret 2000). A deviation from the exponential decay first occurs on MJD 51,695 during observation 11. It is interesting that a flare is seen in the near-IR light curves for XTE J1550−564 that peaks at this time (Jain et al. 2001) and that the radio observation indicating the presence of a compact jet was made soon after on MJD 51,697 (Corbel et al. 2001). A fractionally larger deviation from the exponential decay in the X-ray light curve occurs between MJD 51,710 and 51,730. Generally, the X-ray light curve for XTE J1550−564 is similar to those of other BHC X-ray transients, which typically show reflares, glitches, and secondary maxima (Chen et al. 1997). We note that the ASM data for XTE J1543−568 indicates that it is unlikely that features in the XTE J1550−564 light curve are due to flux variations from the pulsar.

The *Chandra* observations were made on MJD 51,777.405 (2000 August 21) and MJD 51,798.245 (2000 September 11) using the Advanced CCD Imaging Spectrometer (ACIS). We used one of the back-illuminated ACIS chips (S3) to obtain the best low-energy response. For the first observation, a 1.5–12 keV flux of 1.2×10^{-13} ergs cm^{-2} s^{-1} is inferred (assuming an absorbed power-law model), while the flux was 2.5×10^{-13} ergs cm^{-2} s^{-1} for the second observation. The fact that the flux increased by a factor of more than 2 between the observations indicates that the main part of the decay had ended by the time the *Chandra* observations were made. This is consistent with the optical behavior of the source. XTE J1550−564 reached optical quiescence by MJD 51,750 and remained at its quiescent level during both of our *Chandra* observations (Jain et al. 2001).

3. *CHANDRA* ANALYSIS AND RESULTS

We analyzed the data from the *Chandra* observations using the CIAO v2.1 and XSPEC v11.0 software packages. XTE J1550−564 is clearly detected in both observations at R.A. = $15^h50^m58^s.65$, decl. = $-56°28'35''.2$ (equinox 2000.0) with an uncertainty of 1″, which is consistent with the optical and radio positions previously reported (Jain et al. 1999; Corbel et al. 2001). We extracted source spectra for each observation from a circular region with a radius of 5″ and background spectra from an annulus with an inner radius of 5″ and an outer radius of 18″ centered on the source. The outer radius is constrained by the presence of a nearby source. For the first observation, there are brief time segments where excess background is observed. Removing these causes a drop in the exposure time from 5099 to 4985 s. Periods of high background are not seen in the second observation, allowing us to use the entire 4572 s. In the energy band used for spectral analysis (0.5–7 keV), 71 and 111 counts were collected in the source region for the first and second observations, respectively. We determined that the expected background levels in the source extraction region in the 0.5–7 keV energy band are 1.2 and 1.3 counts for the first and second observations, respectively, indicating that background subtraction is unnecessary. The CIAO routine *psextract* was used to extract the spectra and create response matrices. It is important to note that the response matrices created by this routine do not account for the energy dependence of the High-Resolution Mirror Array (HRMA) point-spread function (PSF). This leads to underestimating the source flux, especially at higher energies where the PSF is broader. To correct the response matrix for this effect, we used the HRMA calibration data from Table 4.2 of the *Chandra* Proposer's Guide (10″ diameter case). The data was interpolated to obtain a value for the encircled energy fraction for each energy bin in the ACIS response matrix, and the correction was applied by multiplying the effective areas used for the response matrix by these fractions. For our 5″ extraction radius, the correction causes an increase of the 0.5–7 keV energy flux (and thus the quoted luminosities) by 5%. It should be noted that this correction becomes significantly larger if small extraction radii are used.

We began by fitting each spectrum with a power-law model, which is commonly used for fitting BHC X-ray transients at low flux levels (e.g., Asai et al. 1998). We included interstellar absorption and left the column density as a free parameter. Although the flux is different by a factor of 2 between observations, the spectral parameters obtained are not significantly different, and we carried out further spectral analysis after combining the data for the two observations. The increase in flux for the second observation is rather surprising, and we made light curves for the two observations with four and eight time bins to determine whether the flux increase was caused by a short-timescale phenomenon (e.g., a flare). We found no statistically significant variability in either observation.

We rebinned the spectrum for the two observations combined as shown in Figure 2 and fitted the spectrum using χ^2

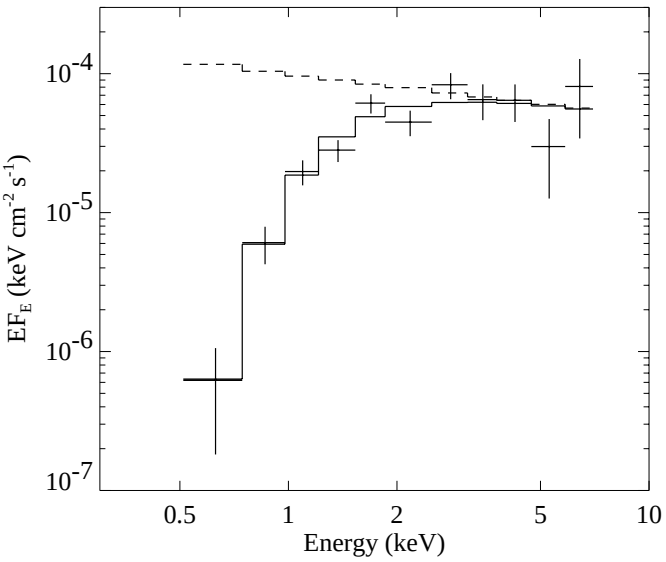

FIG. 2.—The *Chandra*/ACIS energy spectrum for the two *Chandra* observations combined. Solid line is a power law with interstellar absorption, and dashed line is a power law with $\Gamma = 2.3$ without absorption.

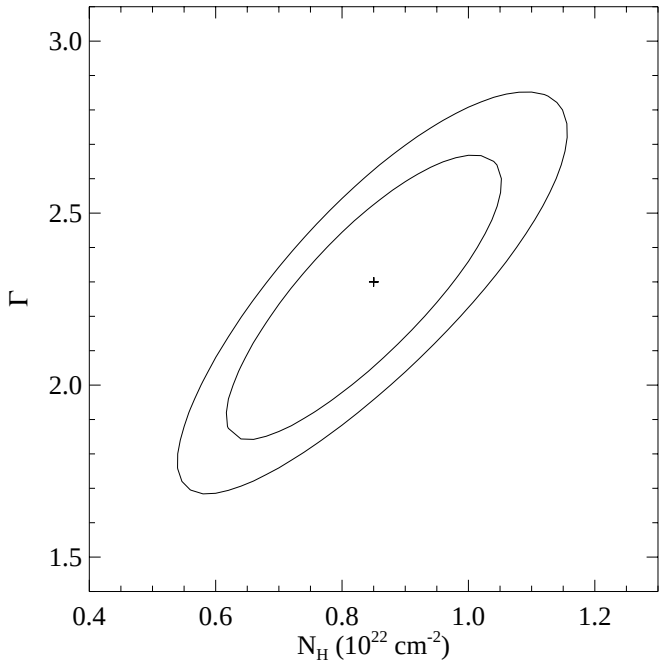

FIG. 3.—Error contours for the column density (N_H) and the power-law index (Γ) derived from the *Chandra* spectrum. The cross marks the location of the best-fit values, and the 68% ($\Delta\chi^2 = 2.30$) and 90% ($\Delta\chi^2 = 4.61$) confidence contours are shown.

minimization first with a power-law model and then with a simple blackbody (both with absorption). The fit is somewhat better for the power-law model ($\chi^2/\nu = 9.5/8$) than for the blackbody model ($\chi^2/\nu = 12.8/8$). In addition, a blackbody temperature of 0.7 keV is obtained, which is considerably higher than typical values seen for quiescent neutron star transients (Asai et al. 1998). The distance for XTE J1550−564 has been estimated at between 2.5 kpc (Sánchez-Fernández et al. 1999) and 6 kpc (Sobczak et al. 1999). For the flux observed during the *Chandra* observations, a blackbody temperature of 0.7 keV implies a blackbody radius of between 0.06 and 0.15 km for distances of 2.5 and 6 kpc, respectively, indicating that it is unlikely that a blackbody interpretation could be physically meaningful. These findings are consistent with the identification of XTE J1550−564 as a black hole rather than as a neutron star system, and in the following we focus on the power-law model.

We refitted the spectrum for the two observations combined with a power-law model with interstellar absorption using the Cash statistic (Cash 1979). This maximum likelihood method allows for the determination of errors and confidence intervals for parameters and does not require that the data be rebinned in energy. This is desirable since rebinning data necessarily removes spectral information. We obtain values of $\Gamma = 2.30^{+0.41}_{-0.48}$ for the power-law photon index and $N_H = (8.5^{+2.2}_{-2.4}) \times 10^{21}$ cm^{-2} for the column density (90% confidence errors are given in both cases). We note that the correction for the energy dependence of the PSF described above changes Γ by only 2%, which is insignificant compared to the statistical errors. Figure 3 shows the 68% and 90% error contours for the two parameters. The column density is consistent with 9×10^{21} cm^{-2}, which is the value for the Galactic column density along the line of sight (Jain et al. 1999), but it is only marginally consistent with the value inferred from the optical work of Sánchez-Fernández et al. (1999). From optical spectra of XTE J1550−564 taken during outburst, they find that $E(B-V) = 0.70 \pm 0.10$, which corresponds to a column density of $(3.9 \pm 0.6) \times 10^{21}$ cm^{-2} (Predehl & Schmitt 1995). The value of N_H measured by *Chandra* could indicate that the distance to the source is somewhat greater than 2.5 kpc, which is the distance estimate obtained from the measured value of $E(B-V)$. The significance of the value we find for Γ is discussed below.

4. *RXTE* SPECTRAL ANALYSIS AND RESULTS

We produced Proportional Counter Array (PCA) and High-Energy X-Ray Timing Experiment (HEXTE) energy spectra for each observation (see Bradt, Rothschild, & Swank 1993 for instrument descriptions). We used the PCA in the 3–25 keV energy band and HEXTE in the 18–150 keV energy band. For the PCA, we used standard-mode data consisting of 129 bin spectra with 16 s time resolution, included the photons from all three anode layers, and estimated the background using the "Sky-VLE" model. For each observation, data was combined from Proportional Counter Units (PCUs) 1–4 that were turned on. For most of the observations, at least one of the PCUs was turned off. Damage to PCU 0 prevented us from using data from this detector. We produced HEXTE energy spectra using standard-mode data, consisting of 64 bin spectra with 16 s time resolution. We used the 1997 March response matrices and applied the necessary dead-time correction (Rothschild et al. 1998). For the spectral fits, the normalization was left free between HEXTE and the PCA. The HEXTE background subtraction is performed by alternating between observations of source and background fields. Each cluster has two background fields, and we checked the background subtraction by comparing the count rates for the two fields.

For the PCA, we used the 2001 February response matrices and tested them by combining spectra from all the available Crab observations from 2000 May 14 to 2001 January 28, where PCUs 1–4 were turned on, resulting in a Crab spectrum with an exposure time of 17,584 s. We fitted the spectrum with a model consisting of two power-law

components, representing the contributions from the nebula and the pulsar, with interstellar absorption. We fixed the column density to 3.2×10^{21} cm^{-2} (Massaro et al. 2000) and the photon index for the pulsar component to 1.8 (Knight 1982). We restricted the bandpass to 3–25 keV since very large residuals (near or above the 5% level) are present outside this range. Even when only the 3–25 keV range is used, we obtain a reduced χ^2 well above 1.0 due to the small statistical errors. The Crab residuals are larger below 8 keV than above this energy, and including 0.8% systematic errors from 3–8 keV and 0.4% systematic errors from 8–25 keV leads to a drop in the reduced χ^2 to 1.0. We added these systematic errors to the XTE J1550−564 spectra to account for uncertainties in the PCA response.

We determined which spectral model to use by fitting the PCA plus HEXTE energy spectrum for observation 1. A power law alone (with interstellar absorption) provides a very poor fit with $\chi^2/\nu = 1118/90$. Large positive residuals are seen near 6–7 keV, and a broad minimum centered near 10 keV is present in the residuals. Models with cutoffs at high energies, such as the Comptonization model of Titarchuk (1994), give even worse fits ($\chi^2/\nu = 1649/88$) since the spectrum extends to high energies without a clear cutoff. We obtain a significant improvement in the fit to $\chi^2/\nu = 135/87$ by adding a smeared iron edge (Ebisawa et al. 1994) to the power law. The smeared edge has been used by other authors to fit XTE J1550−546 spectra (Sobczak et al. 2000) and also for other BHC transients during outburst decay (Tomsick & Kaaret 2000). Even with the smeared edge, large residuals are present below 4 keV, suggesting the presence of a soft component. The addition of a disk-blackbody model (Makishima et al. 1986) with a temperature near 0.5 keV improves the fit significantly to $\chi^2/\nu = 71/85$. Finally, the addition of a Gaussian iron line improves the fit to $\chi^2/\nu = 59/82$, which is significant at the 99.8% level based on an F-test. Although we left all the model parameters free for these fits, the data is not adequate to provide good constraints on the column density, the width of the smeared edge, the line energy or the line width, and, for subsequent fits, we fixed these parameters as follows. We used a value of 9×10^{21} cm^{-2} for the column density, which is the Galactic column density along the line of sight to XTE J1550−564 and is also consistent with the value found using *Chandra*. Following Sobczak et al. (2000), we fixed the width of the smeared edge to 7 keV and the width (σ) of the iron line to 0.5 keV. Also, we fixed the line energy to 6.5 keV, which is consistent with the Kα line for moderately ionized iron. We note that all these values fall within the 68% confidence error regions for the parameters when they are left free and that we obtain $\chi^2/\nu = 63/86$ when the parameters are fixed. Figure 4 shows the observation 1 spectrum and the residuals for a model consisting of a power law, a disk-blackbody, a smeared edge, and an iron line with the parameters fixed as specified above.

We used the same model to fit the other XTE J1550−564 observations. The model provides a good description of the spectrum in each case, with reduced χ^2 values between 0.56 and 1.26 for between 54 and 87 degrees of freedom. We include results only for observations 1–13 because the contamination from the Galactic ridge and the pulsar XTE J1543−568 provides a significant source of uncertainty in parameter estimation for later observations. F-tests indicate that the disk-blackbody is detected only at extremely high

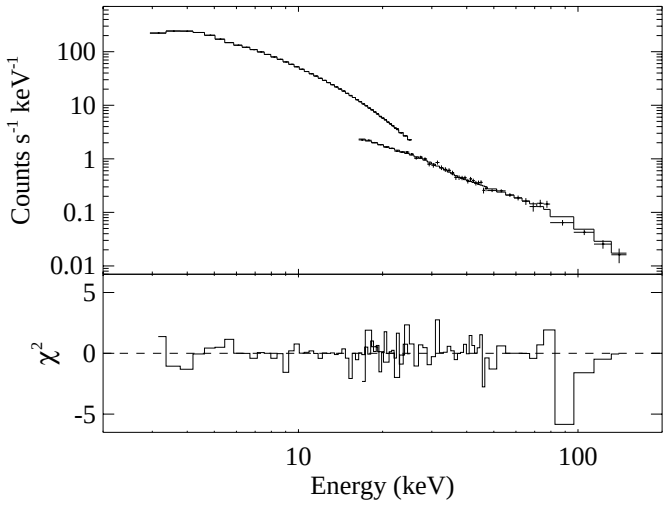

FIG. 4.—*RXTE* energy spectrum for observation 1, including the PCA from 3 to 25 keV and HEXTE from 18 to 150 keV. *Bottom panel*: The residuals in the form of the contribution to the value of χ^2 for each energy bin.

significance $[1-(2 \times 10^{-15})]$ for the first observation. It is marginally detected at 98% confidence for the second observation, and is not statistically significant for the other observations. Inner disk temperatures ($kT_{\rm in}$) of 0.70 and 0.62 keV are obtained for observations 1 and 2, respectively. Although the statistical error on the temperature measurements is 0.05 keV, there is also a systematic uncertainty related to the fact that $kT_{\rm in}$ depends on the column density. We estimate that the total error on the temperature measurements for observations 1 and 2 is near 0.1 keV. The disk-blackbody normalizations[1] are 533^{+202}_{-147} and 355^{+1145}_{-210} for observations 1 and 2, respectively. As for the temperature, the 68% confidence statistical errors reported here underestimate the true normalization uncertainties. Although the disk-blackbody component is not detected at high significance for observations 3–13, we obtain values of $kT_{\rm in}$ near 0.35 keV for observations 3 and 4 with this component in the model. In fitting the spectra for observations 3–13, we included a disk-blackbody component with the temperature fixed to 0.35 keV. At such a low temperature, this component contributes only to the lowest two or three PCA energy bins and does not significantly change the values for the other fit parameters. For observations 3–5, we calculate 90% confidence upper limits on N between 9000 and 15,000, and for observations 6–13, the upper limits are between 1000 and 2100.

The smeared edge is detected at greater than 99% confidence for all observations except for 11 and 13. The edge energies are consistent with neutral or moderately ionized iron and the optical depth of the edge (Ebisawa et al. 1994) drops over time from 0.9 for observation 1 to about 0.4 for observations 8, 9, 10, and 12. However, we emphasize that the smeared edge model is phenomenological, and physical significance should not be attached to its parameters. The feature itself is clearly present in most of the spectra and may be related to Compton reflection (Lightman & White 1988). For most of the observations, the iron line equivalent

[1] The disk-blackbody normalization is $N = \cos i (R_{\rm in}/d_{10})^2$, where i is the binary inclination, $R_{\rm in}$ is the accretion disk inner radius in units of km, and d_{10} is the source distance in units of 10 kpc.

TABLE 2

RXTE Measurement of Power-Law Photon Index (Γ)

Observation	PCA[a]	HEXTE[a]	PCA + HEXTE[a] (No Cutoff)	PCA + HEXTE[a] (With Cutoff)	Consensus[b]
1	2.047 ± 0.012	1.997 ± 0.022	2.053 ± 0.010	...	2.05 ± 0.04
2	1.864 ± 0.013	1.849 ± 0.020	1.878 ± 0.011	1.852 ± 0.014	1.85 ± 0.04
3	1.717 ± 0.005	1.698 ± 0.013	1.720 ± 0.005	1.714 ± 0.004	1.71 ± 0.04
4	1.698 ± 0.006	1.674 ± 0.023	1.700 ± 0.006	1.696 ± 0.005	1.70 ± 0.04
5	1.669 ± 0.005	1.580 ± 0.021	1.665 ± 0.005	...	1.67 ± 0.04
6	1.640 ± 0.008	1.597 ± 0.025	1.637 ± 0.007	...	1.64 ± 0.04
7	1.606 ± 0.007	1.578 ± 0.023	1.606 ± 0.007	...	1.61 ± 0.04
8	1.609 ± 0.008	1.601 ± 0.027	1.609 ± 0.007	...	1.61 ± 0.04
9	1.591 ± 0.013	1.634 ± 0.041	1.598 ± 0.012	...	1.60 ± 0.04
10	1.599 ± 0.018	1.469 ± 0.053	1.581 ± 0.016	...	1.58 ± 0.05
11	1.640 ± 0.018	1.559 ± 0.070	1.632 ± 0.017	...	1.63 ± 0.05
12	1.620 ± 0.012	1.627 ± 0.065	1.620 ± 0.012	...	1.62 ± 0.05
13	1.718 ± 0.021	1.629 ± 0.171	1.726 ± 0.033	...	1.73 ± 0.06

[a] The 68% confidence errors are given.

[b] Measured value for Γ with PCA and HEXTE after accounting for the high-energy cutoffs detected for observations 2, 3, and 4. The error given includes the systematic error (see text).

widths are between 15 and 75 eV; the highest equivalent width of 110 eV occurs for observation 13. The detection significance for the line is greater than 99% for six of the observations.

One of our main results is the evolution of the power-law index during the decay of the outburst. Table 2 shows the photon index for the 13 observations using the PCA alone, the HEXTE alone, and both instruments combined. In all cases, the photon index is near 2.0 for observation 1, but it gradually drops to about 1.6 during the next few observations. We fitted the spectra for the two instruments separately to obtain an estimate of the systematic error due either to the model we are using for the low-energy portion of the spectrum or to uncertainty in the cross calibration between PCA and HEXTE. Although the differences between the PCA and HEXTE are only statistically significant for a few observations, it is clear that there is a systematic effect since the index measured by the PCA is softer than the index measured by HEXTE in 11 of the 13 observations. We estimate the systematic error in the measurement of the photon index by calculating the weighted average of the differences between the PCA and HEXTE. This gives a value of 0.03, which we adopt as the systematic error on the measurement of the power-law index.

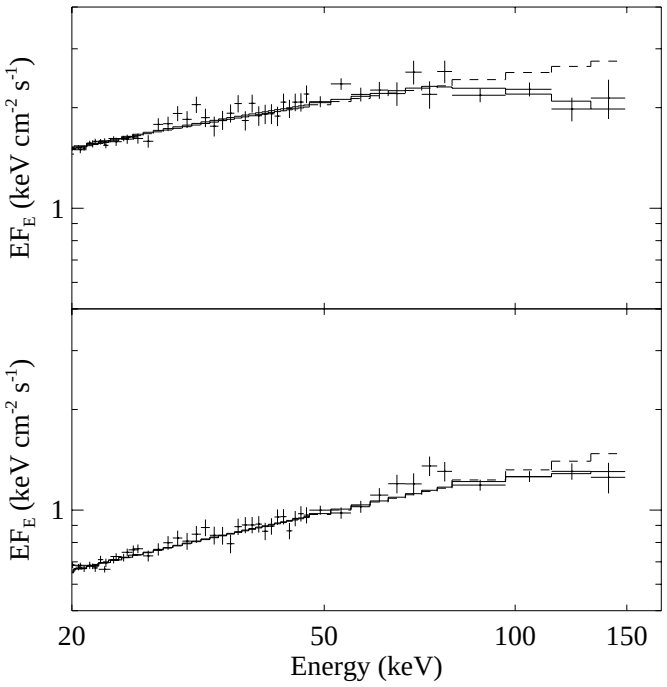

FIG. 5.—High-energy portions of the *RXTE* spectra for observation 3 (*top panel*) and observations 5–12 combined (*bottom panel*). In both cases, the dashed line shows the fit to the spectrum using a power law with no high-energy cutoff, and the solid line shows the fit using a power law with a high-energy cutoff. It is clear that a more significant cutoff is present for observation 3, during the state transition, than for observations 5–12, when the source was in the hard state.

Although the spectral model described above provides satisfactory fits to the energy spectra, for a few of the observations the spectra appear to break in the HEXTE band. To determine whether the breaks are statistically significant, we added a high-energy cutoff to our model and refit the PCA/HEXTE energy spectra. We used the XSPEC model *highecut*, which has two free parameters and has been used previously by several authors to model spectral breaks (e.g., Grove et al. 1998). Including this model modifies the power law for energies above $E_{\rm cut}$, producing an exponential cutoff with an *e*-folding energy $E_{\rm fold}$, but does not alter the spectrum for energies below $E_{\rm cut}$. For observations 2, 3, and 4, *F*-tests show that the cutoff is significant at 99.8% confidence or greater, but the cutoff is less significant for the other observations. The cutoff is detected at extremely high

TABLE 3

Break Parameters for the *RXTE* Spectra

Observation	$E_{\rm cut}$[a] (keV)	$E_{\rm fold}$[a] (keV)
2	40^{+8}_{-7}	338^{+91}_{-83}
3	72^{+8}_{-9}	194^{+71}_{-48}
4	73^{+10}_{-18}	175^{+110}_{-57}
5–12	78^{+23}_{-11}	462^{+342}_{-241}

[a] The 68% confidence errors are given.

significance [$1-(2.6 \times 10^{-8})$] only for observation 3. Table 2 includes the measurement of the photon index when the break is included for observations 2, 3, and 4. The change in photon index is not significant for any of the observations. We combined the data from observations 5–12, all of which have the same value for Γ within errors, and refitted the PCA/HEXTE spectrum with and without a cutoff. Adding a cutoff provides a marginally significant (98% confidence) improvement, indicating that the break is weak in this case if it is present. The best-fit values for $E_{\rm cut}$ and $E_{\rm fold}$ are given in Table 3 for observations 2, 3, 4, and 5–12. Figure 5 shows the high-energy portion of the spectrum for observation 3, where the most significant cutoff is detected, and for observations 5–12.

5. DISCUSSION

5.1. *Transition to the Hard State*

The spectral evolution we observe during the *RXTE* observations shows that XTE J1550−564 was in the process of making a transition to the hard state as our observations began. Figure 6 shows the evolution of the power-law photon index (Γ) for the *RXTE* and *Chandra* observations. The drop in Γ during the first few *RXTE* observations along with the timing properties reported in Paper II indicate that the source made a transition to the hard state. In addition, the drop in temperature and eventual nondetection of the soft component is common when such transitions occur (see Tomsick & Kaaret 2000 and references therein). Although our observations do not provide information about the state of the source before the transition, Corbel et al. (2001) indicate that XTE J1550−564 was in the intermediate/very high state before the transition since relatively strong hard X-ray emission was observed by the Burst and Transient Source Experiment (BATSE) on board the *Compton Gamma-Ray Observatory* (*CGRO*) throughout the outburst. Observations of XTE J1550−564 made during the rise of the 1998–1999 outburst indicate also that the source made a transition from the hard state to the intermediate/very high state (Cui et al. 1999; Wilson & Done 2001).

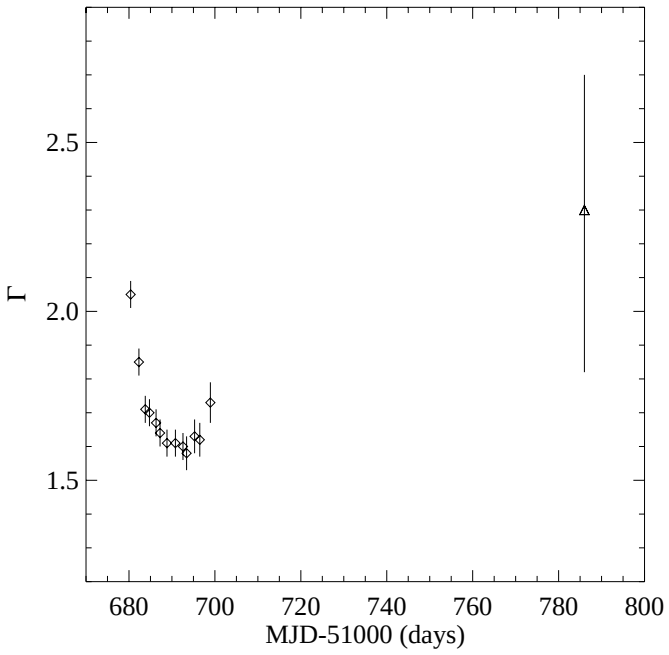

FIG. 6.—The evolution of the power-law index (Γ) for the pointed *RXTE* observations (*diamonds*) and the combination of the two *Chandra* observations (*triangle*). The *RXTE* values come from the last column of Table 2, and the error bars shown include the systematic error discussed in the text. For the *Chandra* point, a 90% ($\Delta\chi^2 = 2.71$) confidence error bar is shown.

XTE J1550−564 is one of the few BHC X-ray transients that has had multiple outbursts, allowing us to compare the source behavior during the 2000 decay to that of the previous outburst. For the 2000 outburst, the transition to the hard state occurred when the source was still relatively bright. The flux for the second *RXTE* observation, which is probably near the midpoint of the transition, is 5×10^{-9} ergs cm^{-2} s^{-1} (3–25 keV). The previous outburst was observed with *RXTE* to a flux level over an order of magnitude lower (Sobczak et al. 2000). Although the behavior of the soft component shows some similarities between the two outbursts, the evolution of the power-law component was completely different. In contrast to the 2000 decay, Γ remained at between 2.2 and 2.6 down to a 2–20 keV flux level of 5×10^{-10} ergs cm^{-2} s^{-1} for the previous outburst. The subsequent observations showed some hardening of the power-law component, but the energy spectrum did not show clear evidence for a transition to the hard state. For both outbursts, a disk-blackbody component with an inner disk temperature of 0.6–0.7 keV was present when the source flux was near 6×10^{-9} ergs cm^{-2} s^{-1}, and in both cases, a drop in temperature occurred as the source decayed. As discussed by Sobczak et al. (2000), the evolution of the soft component could indicate an increase in the inner radius of the accretion disk. If this is the case, it is likely that the inner radius increased more rapidly with flux for the 2000 decay than for the previous decay since the soft component was detected down to very low flux levels during the 1998–1999 decay, while we did not detect the soft component after observation 2.

We also used *RXTE* to monitor the BHC X-ray transient 4U 1630−47 during the decay of its 1998 outburst (Tomsick & Kaaret 2000). The source made a transition to the hard state, and we observed 4U 1630−47 several times during the transition, making it interesting to compare its behavior to that of XTE J1550−564. For 4U 1630−47, Γ hardened from 2.3 to 1.8 over a period of 8 days, and the soft component became undetectable during the transition. Although our observations did not include the beginning of the XTE J1550−564 transition, Γ changed from 2.05 to 1.67 in 3.4 days, suggesting that the transition timescale is similar for the two sources. The estimated transition luminosities are similar for the two sources. Taking the second XTE J1550−564 observation as the midpoint of the transition and assuming isotropic X-ray emission gives a transition luminosity of 9×10^{36} ergs s^{-1} (3–25 keV, unabsorbed). As mentioned above, distance estimates for XTE J1550−564 range from 2.5 to 6 kpc, and here we adopt a distance of 4 kpc. For 4U 1630−47, we estimated a transition luminosity of 7×10^{36} ergs s^{-1} (2.5–20 keV).

5.2. *Spectral Evolution after the Hard-State Transition*

After the source made a transition to the hard state, Figure 6 shows that the power-law index remained very close to 1.6 until the last *RXTE* observation, where Γ showed a marginally significant increase to 1.73 ± 0.06. Although statistical significance of the change is not high,

spectral softening at low luminosities is predicted if an ADAF is present (Esin, McClintock, & Narayan 1997) since the X-ray emission is dominated by inverse Comptonization from the thermal distribution of electrons in the ADAF region. As the mass accretion rate drops, the predicted spectrum gradually softens since the optical depth of the ADAF region decreases, leading to a decrease in the Compton y-parameter. The *Chandra* spectrum provides evidence for further softening at low luminosities, which is also a prediction of the ADAF model. As shown in Figure 6, the lower limit on Γ for the *Chandra* observation is 1.82 based on the 90% confidence error bars, representing reasonably good evidence for spectral softening.

Although there is evidence that spectral evolution occurred for XTE J1550−564 between the *RXTE* observations and the *Chandra* observations, it is not clear whether this evolution occurred gradually (as predicted by ADAF models) or suddenly as the source flux decayed. In fact, not many X-ray observations of BHC systems have been made in the luminosity gap between our last *RXTE* observation, where the 3–25 keV luminosity was 9.6×10^{35} ergs s^{-1}, and our *Chandra* observations, where the mean unabsorbed 0.5–7 keV luminosity was 6.7×10^{32} ergs s^{-1}, and only a few of these observations have produced useful energy spectra. *BeppoSAX* observations of the BHC GX 339−4 at 7×10^{33} ergs s^{-1} indicate that it remains relatively hard ($\Gamma = 1.64 \pm 0.13$) at low luminosity (Kong et al. 2000). Similarly, an *Advanced Satellite for Cosmology and Astrophysics* (*ASCA*) observation of XTE J1748−288 at a luminosity of 4×10^{35} ergs s^{-1} (assuming a distance of 8.5 kpc) gave $\Gamma = 1.56^{+0.34}_{-0.31}$ (Kotani et al. 2000). However, *Ginga* observations of GS 1124−68 show some evidence for spectral softening. A power-law index of $\Gamma = 1.84^{+0.03}_{-0.04}$ was measured at a source luminosity of 5×10^{34} ergs s^{-1} (assuming a distance of 2.5 kpc), even though $\Gamma = 1.5$ was obtained when the source was brighter. V404 Cyg is the one BHC X-ray transient with a quiescent luminosity higher than the XTE J1550−564 luminosity during our *Chandra* observations (Garcia et al. 2001). This source has been observed in quiescence at a luminosity near 10^{33} ergs s^{-1} by both *ASCA* and *BeppoSAX*, and power-law indices of $2.1^{+0.5}_{-0.3}$ (Narayan, Barret, & McClintock 1997), $1.7^{+0.3}_{-0.2}$ (Asai et al. 1998), and $1.9^{+0.6}_{-0.5}$ (Campana, Parmar, & Stella 2001) have been reported. This provides some evidence for spectral softening at low luminosities since values of Γ between 1.3 and 1.5 were observed for V404 Cyg during outburst (Tanaka & Lewin 1995).

The results discussed in the previous paragraph appear to indicate that the evolution of Γ as the luminosity decreases is not consistent from source to source. Spectral softening is observed for GS 1124−68 and is probably observed for XTE J1550−564 and V404 Cyg, while the observations show that the spectra of GX 339−4 and XTE J1748−288 remain hard down to relatively low luminosities. The latter type of behavior is difficult to explain with the ADAF model, but such behavior can be explained if the X-ray emission is due to magnetic flares above the disk (Galeev et al. 1979; di Matteo, Celotti, & Fabian 1999). In fact, a magnetic flare model has been used to explain the spectral evolution of GX 339−4 (di Matteo et al. 1999). A sharp transition to a quiescent state would be expected if the emission in the hard state is due to magnetic flares. This is because the MHD turbulence that is responsible for the magnetic flares (Balbus & Hawley 1991) is expected to turn off when the accretion disk temperature drops (Gammie & Menou 1998). Other accretion physics may also be important at low luminosities that will alter the X-ray emission properties. For low-viscosity accretion flows, theory and simulations show that convection plays an important role (Narayan, Igumenshchev, & Abramowicz 2000). In the X-ray band, convection-dominated accretion flows (CDAFs) produce most of their emission via thermal bremsstrahlung in contrast to the mechanisms at work for the ADAF and magnetic flare models. Rather than being a pure power law, CDAF models predict that a peak will be observed in the X-ray band (Ball, Narayan, & Quataert 2001). Although the XTE J1550−564 *Chandra* spectrum does not show evidence for such a peak, the statistical quality of the data does not allow us to rule this out either.

The radio observations of XTE J1550−564 during the 2000 outburst give evidence for the presence of a compact jet only after the transition to the hard state (Corbel et al. 2001). An inverted radio spectrum was observed on MJD 51,697.14 within a day of observation 12. Multiwavelength observations suggest that the synchrotron emission from the jet extends from the radio to at least the near-IR and optical range, indicating a very powerful compact jet (Corbel et al. 2001). None of the models discussed here (ADAF, CDAF, and magnetic flares) include outflows required to produce such a jet. Further theoretical modeling, including outflows, would be of great interest to allow a comparison with the broadband (radio, IR, optical, and X-ray) behavior of the source. This is currently under investigation for BHC systems in the hard state (e.g., Markoff, Falcke, & Fender 2001).

5.3. *XTE J1550−564 and X-Ray Transients at Low Luminosities*

X-ray observations of transient systems in quiescence suggest that, for a given mass accretion rate, black hole systems are significantly less luminous than neutron star systems (Garcia et al. 2001). Since the ADAF model interprets this as being due to the presence of an event horizon for the black hole systems (Narayan et al. 1997), it is important to establish this trend using as many systems as possible, and it is interesting to compare the minimum luminosity we observe for XTE J1550−564 to the quiescent luminosities of other transients. During our first *Chandra* observation, the unabsorbed 0.5–7 keV luminosity was between 2×10^{32} and 1.2×10^{33} ergs s^{-1} based on the 2.5–6 kpc distance range. Although XTE J1550−564 is an established black hole system, this range of luminosities is comparable to neutron star systems and is 25–150 times brighter than the median quiescent black hole luminosity for detections given in Garcia et al. (2001). While this could have important implications for the question of whether the quiescent luminosities of black holes and neutron stars are different, we believe that it is unlikely that the system was in true quiescence during our *Chandra* observations. The luminosity increase observed for our second *Chandra* observation and the minioutburst that occurred about 4 months later both suggest the continuation of significant variability in the mass accretion rate. Perhaps XTE J1550−564 will prove to be similar to GRO J1655−40, which was detected at relatively high X-ray luminosity between two outbursts but was later observed by *Chandra* with an order of magnitude lower luminosity. Since our observations provide only an upper limit on the true quiescent luminosity, future

X-ray observations of XTE J1550−564 are necessary to determine this quantity.

The *Chandra* spectrum for XTE J1550−564 provides an opportunity for comparison to the neutron star system Cen X-4. This comparison is especially useful because Cen X-4 was observed with the same instrument (ACIS back-illuminated chip) at a luminosity within a factor of a few of XTE J1550−564 (Rutledge et al. 2001). A soft component and a power law are necessary to fit the Cen X-4 spectrum in contrast to XTE J1550−564, where the spectrum requires only one component. It is very likely that the Cen X-4 soft component is thermal emission from the surface of the neutron star, and it can be modeled as a blackbody with a temperature of 0.175 keV. Using fit parameters from Rutledge et al. (2001), the blackbody component contributes 62% of the total 0.5–7 keV unabsorbed flux for Cen X-4. Although a two-component model does not improve the fit for XTE J1550−564, we fitted the spectrum with a blackbody plus power-law model to make a more direct comparison with Cen X-4. The blackbody parameters are not well constrained for XTE J1550−564, and we fixed the temperature to 0.175 keV to calculate an upper limit on the blackbody flux. The 90% confidence upper limit on the ratio of the blackbody flux to the total 0.5–7 keV unabsorbed flux is 32%, which is significantly lower than the measured value for Cen X-4. Finally, we note that the Cen X-4 power-law component has a photon index of $1.2^{+0.4}_{-0.5}$, which is considerably harder than the power law observed for XTE J1550−564. We conclude that the Cen X-4 and XTE J1550−564 spectra are significantly different and speculate that this is related to the fact that one contains a neutron star while the other contains a black hole.

5.4. *High-Energy Cutoff*

Our results indicate that the high-energy cutoff for XTE J1550−564 is stronger in the HEXTE band during the state transition (observations 2, 3, and 4) than after the source reaches the hard state (observations 5–12). It may be possible to explain this in the context of the standard picture that the hard X-ray emission is due to inverse Comptonization of soft photons by thermal electrons where the measured folding energy ($E_{\rm fold}$) is close to the electron temperature. In this picture, the lower value of $E_{\rm fold}$ during the transition indicates a lower electron temperature during the transition than in the hard state. The temperature change could be related to the observed drop in the strength of the soft component during the transition to the hard state since a drop in soft-photon cooling would lead to a higher temperature for the Comptonizing electrons. However, the lack of a significant cutoff for observation 1 is a problem for this picture since the strongest soft component is seen in this case. A different mechanism, such as bulk-motion Comptonization (Chakrabarti & Titarchuk 1995), may be necessary to explain the hard X-ray emission seen during observation 1. The possibility that both these mechanisms may operate in accreting BHCs has been discussed previously by several authors (e.g., Ebisawa, Titarchuk, & Chakrabarti 1996).

The folding energy we obtain for observations 5–12 ($E_{\rm fold} = 462^{+342}_{-241}$ keV, 68% confidence errors) is high compared to the folding energies reported by Grove et al. (1998) for accreting BHCs in the hard state, which are between 87 and 132 keV. Since it is thought that the high-energy emission in the hard state is produced via thermal Comptonization, this raises the question of whether realistic accretion disk models can be constructed with high enough electron temperatures to give the values of $E_{\rm fold}$ we observe for XTE J1550−564. Detailed comparisons between ADAF predictions and the XTE J1550−564 spectra will be a subject of future work, but a preliminary result is that the ADAF model underpredicts the level of high-energy emission (Esin & Tomsick 2001). Emission mechanisms other than thermal Comptonization may be required to explain the high-energy emission such as Comptonization from a nonthermal electron distribution or possibly synchrotron emission (Markoff, Falcke, & Fender 2001). Since the compact jet is a possible source of high-energy emission, correlations between hard X-ray emission and radio or IR emission (such as those mentioned in § 2) are especially interesting.

6. SUMMARY AND CONCLUSIONS

We report on spectral analysis of *RXTE* and *Chandra* observations made during the decay of the 2000 outburst from the BHC XTE J1550−564. A rapid and approximately exponential drop in flux was observed early in the decay with an *e*-folding time of 6.0 days. The evolution of the energy spectrum during this time indicates that the system made a transition to the hard state with a drop in the flux of the soft component in the *RXTE* energy band and a hardening of the power law used to model the hard component. The transition occurred near a luminosity of 9×10^{36} ergs s^{-1} assuming a source distance of 4 kpc. The spectral changes, the transition luminosity, and the timescale for the transition are similar to those we have previously observed for another BHC, 4U 1630−47. However, we note that the XTE J1550−564 hard-component behavior was significantly different during the decay of the 1998–1999 outburst.

The mean luminosity during the *Chandra* observations is within a factor of a few of the quiescent luminosity of the neutron star system Cen X-4. In contrast to Cen X-4 (Rutledge et al. 2001), the XTE J1550−564 spectrum is well described by a single power-law component with a photon index (Γ) of $2.30^{+0.41}_{-0.48}$ (90% confidence). Since we measured a value of 1.6 for Γ in the hard state, the *Chandra* spectrum provides reasonably good evidence for spectral softening at low luminosities. ADAF models predict gradual spectral softening as the luminosity drops, but our observations do not allow us to determine whether the spectral evolution is gradual or sudden. Future observations to measure the spectral evolution at intermediate luminosities are important and may allow us to distinguish between ADAF models and magnetic flare models. The lowest luminosity we measure for XTE J1550−564 with *Chandra* is 5×10^{32} ergs s^{-1}. This is probably not the true quiescent luminosity, but it represents a useful upper limit on this quantity.

Although a highly significant break is seen in the HEXTE band for observation 3 during the state transition, the break becomes weaker once the source reaches the hard state. For XTE J1550−564, the hard-state cutoff energy is higher than those found for other BHCs (Grove et al. 1998), and this may indicate the presence of nonthermal emission. More theoretical and observational work is necessary to understand the mechanism responsible for the high-energy emission. Observations of BHC X-ray transients in their hard state with the *International Gamma-Ray Astrophysics Laboratory* (*INTEGRAL*) will be especially useful.

We would like to thank *Chandra* director Harvey Tananbaum for granting Director's Discretionary Time and Jean Swank for assistance with *RXTE* observations. We also thank Raj Jain for providing optical and IR results prior to publication. J. A. T. acknowledges useful discussions with Ann Esin. This material is based upon work supported by the National Aeronautics and Space Administration under grant NAG 5-10886. P. K. acknowledges partial support from NASA grant NAG 5-7405.

REFERENCES

Asai, K., Dotani, T., Hoshi, R., Tanaka, Y., Robinson, C. R., & Terada, K. 1998, PASJ, 50, 611
Balbus, S. A., & Hawley, J. F. 1991, ApJ, 376, 214
Ball, G. H., Narayan, R., & Quataert, E. 2001, ApJ, 552, 221
Bradt, H. V., Rothschild, R. E., & Swank, J. H. 1993, A&AS, 97, 355
Campana, S., Parmar, A. N., & Stella, L. 2001, A&A, 372, 241
Campbell-Wilson, D., McIntyre, V., Hunstead, R., Green, A., Wilson, R. B., & Wilson, C. A. 1998, IAU Circ. 7010
Cash, W. 1979, ApJ, 228, 939
Chakrabarti, S., & Titarchuk, L. G. 1995, ApJ, 455, 623
Chen, W., Shrader, C. R., & Livio, M. 1997, ApJ, 491, 312
Corbel, S., et al. 2001, ApJ, 554, 43
Cui, W., Zhang, S. N., Chen, W., & Morgan, E. H. 1999, ApJ, 512, L43
di Matteo, T., Celotti, A., & Fabian, A. C. 1999, MNRAS, 304, 809
Ebisawa, K., Titarchuk, L., & Chakrabarti, S. K. 1996, PASJ, 48, 59
Ebisawa, K., et al. 1994, PASJ, 46, 375
Esin, A. A., McClintock, J. E., & Narayan, R. 1997, ApJ, 489, 865
Esin, A. A., & Tomsick, J. A. 2001, AAS Meeting, 198, 1001
Galeev, A. A., Rosner, R., & Vaiana, G. S. 1979, ApJ, 229, 318
Gammie, C. F., & Menou, K. 1998, ApJ, 492, L75
Garcia, M. R., McClintock, J. E., Narayan, R., Callanan, P., Barret, D., & Murray, S. S. 2001, ApJ, 553, L47
Grove, J. E., Johnson, W. N., Kroeger, R. A., McNaron-Brown, K., Skibo, J. G., & Phlips, B. F. 1998, ApJ, 500, 899
Hannikainen, D., et al. 2001, in Proc. 4th *INTEGRAL* Workshop, in press (Noordwijh: ESA)
Homan, J., Wijnands, R., & van der Klis, M. 1999, IAU Circ. 7121
Homan, J., et al. 2001, ApJS, 132, 377
Jain, R., Bailyn, C., & Tomsick, J. 2001, IAU Circ. 7575
Jain, R. K., Bailyn, C. D., Orosz, J. A., McClintock, J. E., & Remillard, R. A. 2001, ApJ, 554, L181
Jain, R. K., Bailyn, C. D., Orosz, J. A., Remillard, R. A., & McClintock, J. E. 1999, ApJ, 517, L131
Kalemci, E., Tomsick, J., Rothschild, R., Pottschmidt, K., & Kaaret, P. 2001, ApJ, 563, 239 (Paper II)
Kaptein, R., in't Zand, J. J. M., & Heise, J. 2001, IAU Circ. 7588
Knight, F. K. 1982, ApJ, 260, 538
Kong, A. K. H., Kuulkers, E., Charles, P. A., & Homer, L. 2000, MNRAS, 312, L49
Kotani, T., et al. 2000, ApJ, 543, L133
Lightman, A. P., & White, T. R. 1988, ApJ, 335, 57
Makishima, K., et al. 1986, ApJ, 308, 635
Markoff, S., Falcke, H., & Fender, R. 2001, A&A, 372, L25
Marshall, F. E., Takeshima, T., & in't Zand, J. 2000, IAU Circ. 7363
Massaro, E., Cusumano, G., Litterio, M., & Mineo, T. 2000, A&A, 361, 695
Miller, J., et al. 2001a, MNRAS, submitted
———. 2001b, ApJ, submitted
Narayan, R., Barret, D., & McClintock, J. E. 1997, ApJ, 482, 448
Narayan, R., Garcia, M. R., & McClintock, J. E. 1997, ApJ, 478, L79
Narayan, R., Igumenshchev, I. V., & Abramowicz, M. A. 2000, ApJ, 539, 798
Orosz, J., Bailyn, C., & Jain, R. 1998, IAU Circ. 7009
Orosz, J. A., van der Klis, M., McClintock, J. E., Jain, R. K., Bailyn, C. D., & Remillard, R. A. 2001, Astron. Telegram, 70, 70
Predehl, P., & Schmitt, J. H. M. M. 1995, A&A, 293, 889
Remillard, R. A., McClintock, J. E., Sobczak, G. J., Bailyn, C. D., Orosz, J. A., Morgan, E. H., & Levine, A. M. 1999, ApJ, 517, L127
Remillard, R. A., Sobczak, G. J., Muno, M. P., & McClintock, J. E. 2001, ApJ, submitted
Rothschild, R. E., et al. 1998, ApJ, 496, 538
Rutledge, R. E., Bildsten, L., Brown, E. F., Pavlov, G. G., & Zavlin, V. E. 2001, ApJ, 551, 921
Sánchez-Fernández, C., et al. 1999, A&A, 348, L9
Smith, D. A. 1998, IAU Circ. 7008
Smith, D. A., et al. 2000, IAU Circ. 7399
Sobczak, G. J., McClintock, J. E., Remillard, R. A., Levine, A. M., Morgan, E. H., Bailyn, C. D., & Orosz, J. A. 1999, ApJ, 517, L121
Sobczak, G. J., et al. 2000, ApJ, 544, 993
Tanaka, Y., & Lewin, W. H. G. 1995, X-Ray Binaries (Cambridge: Cambridge Univ. Press)
Titarchuk, L. 1994, ApJ, 434, 570
Tomsick, J. A., & Kaaret, P. 2000, ApJ, 537, 448
Tomsick, J. A., Smith, E., Swank, J., Wijnands, R., & Homan, J. 2001, IAU Circ. 7575
Valinia, A., & Marshall, F. E. 1998, ApJ, 505, 134
van der Klis, M. 1995, X-Ray Binaries (Cambridge: Cambridge Univ. Press)
Wilson, C. D., & Done, C. 2001, MNRAS, 325, 167